Journal

Rhombohedral–Tetragonal Phase Coexistence and Piezoelectric Properties of (NaK)(NbSb)O₃–LiTaO₃–BaZrO₃ Lead-Free Ceramics

Ruzhong Zuo[†] and Jian Fu

Institute of Electro Ceramics & Devices, School of Materials Science and Engineering, Hefei University of Technology, Hefei 230009, China

The phase transitional behavior and composition-dependent piezoelectric properties of (NaK)(NbSb)O₃–LiTaO₃–BaZrO₃ (NKNS–LT–BZ) pseudo-ternary system were investigated. A composition–temperature phase diagram was generalized within a certain range of BZ content in which a rhombohedral–tetragonal (R–T) ferroelectric phase boundary connecting orthorhombic and cubic phase zones is formed near room temperature between two trifurcate points. Piezoelectric and electromechanical properties of NKNS–LT–BZ ceramics exhibit optimum values of d_{33} = 365 pC/N and k_p = 45% in the vicinity of the R–T phase coexistence zone. The dielectric and ferroelectric properties and the phase transition of NKNS–LT–BZ ceramics were discussed from a crystallographic point of view.

I. Introduction

THE (Na₀.₅K₀.₅)NbO₃ (NKN) has been considered as a typical lead-free ferroelectric with a perovskite structure however its complex phase transition behavior has created different features from those of traditional Pb-based perovskite compositions such as PbZrO₃–PbTiO₃ (PZT) or Pb(Mg₁/₃Nb₂/₃)O₃–PbTiO₃ (PMN–PT). From low temperature to high temperature, it undergoes successive phase transitions: rhombohedral to orthorhombic (R–O) transition at ~−123°C, orthorhombic to tetragonal (O–T) transition at ~200°C and tetragonal to cubic (T–C) transition at ~410°C.[1] Like BaTiO₃ (BT), these phase transition temperatures can be adjusted by adding some dopants.[2] The O–T polymorphic phase transition (PPT) temperature (T_{O-T}) has attracted most attention in the last few years mainly because the coexistence of O–T ferroelectric phases led to enhanced piezoelectric and electromechanical properties.[3] The usual way to achieve this feature has been involved in either adding dopants such as Li⁺,[4] Ta⁵⁺,[5] and Sb⁵⁺,[6] or forming solid solutions with compounds such as (Bi₀.₅Na₀.₅)TiO₃,[7] (Bi₀.₅K₀.₅)TiO₃,[8] BiMO₃ (M: Fe³⁺, Sc³⁺, and Al³⁺),[9] and NTiO₃ (N: Ba²⁺, Ca²⁺, Mg²⁺, and Sr²⁺).[10] Only recently, a few new attempts[11,12] have been made to design NKN-based ceramics with the R–O phase coexistence by shifting T_{R-O} toward room temperature. It has been demonstrated that these compositions are still based a polymorphic phase boundary (PPB),[13] rather than a classical morphotropic phase boundary (MPB).

However, traditional Pb-based piezoelectric compositions are usually located in the proximity of the R–T phase coexistence zone. It is thus of interest to ask if it is possible to make NKN-based compositions with R–T phase coexistence. According to the rule of shifting T_{R-O} and T_{O-T} in NKN, it seems reasonable

to create an R–T phase boundary near room temperature only if the O phase zone can be compressed completely. This idea has recently proved to be doable in BT, a similar system to NKN, by adjusting the content of Ca²⁺, Ba²⁺, Zr⁴⁺, and Ti⁴⁺.[14] The purpose of this study is thus to design new NKN-based compositions. BaZrO₃ (BZ) is a paraelectric phase with a cubic perovskite structure and expected to stabilize the R phase of NKN.[11] LiTaO₃ (LT) and LiSbO₃ (LS) seemed to broaden the tetragonal phase zone by shifting T_{O-T} downward.[5,6] It is anticipated that BZ, LT, and LS can be used to tune the phase transition behavior of NKN. The relationship between the phase structural transformation and electrical properties was discussed.

II. Experimental Procedures

A pseudo-ternary lead-free system (Na₀.₅₂K₀.₄₀)(Nb₀.₈₄Sb₀.₀₈)O₃–(0.08–x)LiTaO₃–xBaZrO₃ (NKNS–LT–xBZ) was designed where x is the molar percent of BZ. The samples were prepared by a conventional solid-state reaction method using high-purity carbonates and oxides: Na₂CO₃ (99.8%), K₂CO₃ (99.0%), Li₂CO₃ (99.9%), BaCO₃ (99.0%), Nb₂O₅ (99.5%), Ta₂O₅ (99.9%), Sb₂O₃ (99.9%), and ZrO₂ (99.0%). Specimens were sintered in air in the temperature range of 1080°–1220°C for 3 h. The electric poling was performed at 110°C in a silicone oil bath by applying a dc field of 2–3 kV/mm for 15 min.

The crystal structure of the ceramics was identified by a powder X-ray diffractometer (XRD, D/MAX2500VL/PC, Rigaku, Tokyo, Japan) and a Raman spectrometer (633 nm, LabRAM HR800, HJY, Longjumeau Cedex, France) under ambient and elevated temperature, respectively. The full XRD patterns and {200} profiles were measured by a step width of 0.02°. The dielectric permittivity was measured in the temperature range of −190° and 350°C by an LCR meter (E4980A, Agilent, Santa Clara, CA) equipped with a temperature box. Polarization-electric field (P–E) hysteresis loops were measured using a ferroelectric measuring system (Precision LC, Radiant Technologies Inc., Albuquerque, NM). The piezoelectric coefficient d_{33} and electromechanical properties k_p were measured by a Belincourt meter (YE2730A, Sinocera, Yangzhou, China) and an impedance analyzer (PV70A, Beijing Band ERA Co. Ltd., Beijing, China), respectively.

III. Results and Discussion

Figure 1 shows the crystal structure of NKNS–LT–xBZ solid solutions changing with BZ content x and temperature, as characterized by means of XRD and Raman spectrometry. The typical perovskite structure was identified for all compositions (Fig. 1(a)) and only a trace of the secondary phase can be detected as x is >0.06, probably owing to the lower solubility limit of BZ in NKNS matrix than LT. It can be seen that with increasing BZ content x the crystal structure of samples at room temperature gradually changes from T to R symmetry, as manifested by split peaks of (200) diffraction lines. These (200) diffraction lines were fitted by Gaussian function as shown in Fig. 1(b). It can be found that the integrated intensities of (200)$_R$
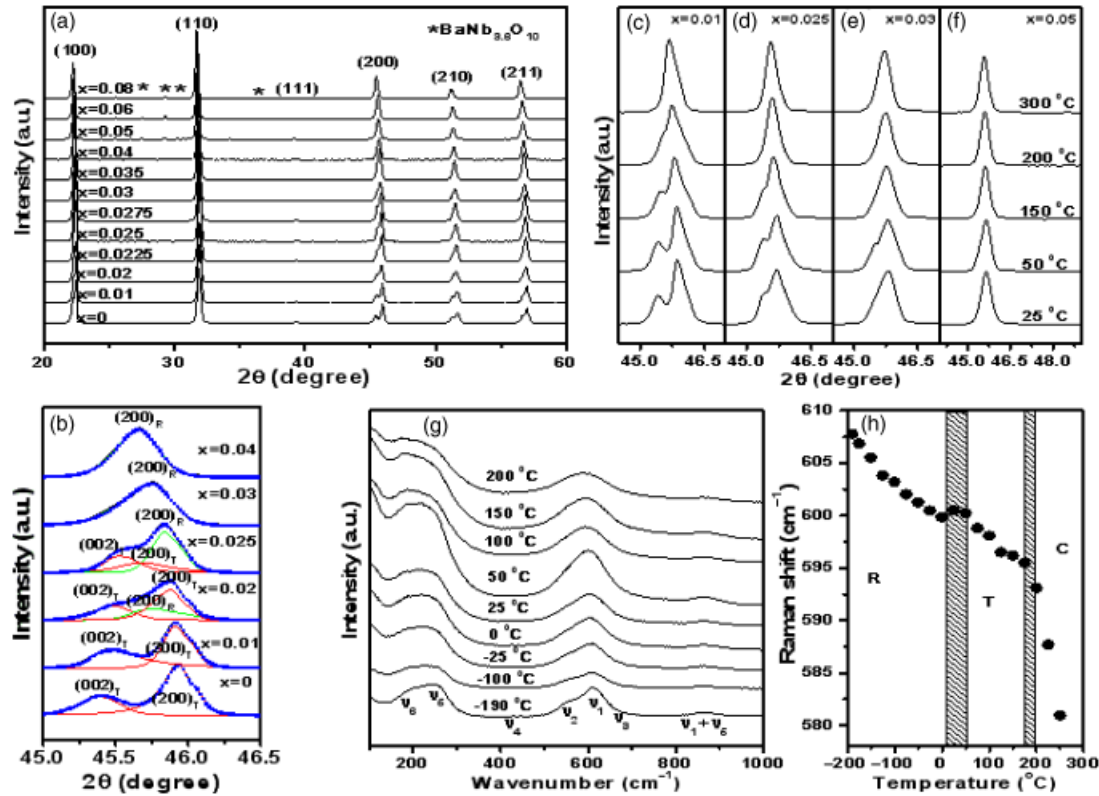
Fig. 1. (a) Powder X-ray diffractometer (XRD) patterns of NKNS–LT–xBZ ceramics, (b) the (200) reflection lines of NKNS–LT–xBZ ceramics fitted with Gaussian function, (c)–(f) XRD profiles for samples with $x = 0.01$, 0.025, 0.03 and 0.05 measured at elevated temperatures as indicated, (g) Raman spectra of NKNS–LT–0.025BZ ceramics measured at various temperatures as indicated, and (h) peak shift for the ν_1 stretching mode as a function of temperature.

increase with an increase of x while the intensities of $(200)_T$ and $(002)_T$ decrease remarkably. Therefore, a two-phase coexistence zone near room temperature consisting of R and T phases can be estimated within $0.02 \leq x \leq 0.03$. Moreover, the structural parameters were refined by the Rietveld method using a Maud software for NKNS–LT–xBZ ceramics from XRD data shown in Fig. 1(a). The lattice parameters, space groups, reliability factor R_{wp}, and the goodness-of-fit indicator S are listed in Table I. The low S values suggest that the assigned structural models to each composition are reasonable. It was found that the structure can be well refined using a tetragonal $P4mm$ model for $x < 0.02$, a rhombohedral $R3m$ model for $x \geq 0.03$ and a coexisting $P4mm$ and $R3m$ model for $0.02 \leq x < 0.03$. Furthermore, the c/a ratio was found to decrease with increasing x and finally becomes unity owing to a T–R phase transition.

Figures 1(c)–(f) indicate the change of the crystal structure with temperature for four different compositions as indicated. It is obvious that the PPT temperatures have been adjusted by the substitution of BZ for LT. For the sample with $x = 0.01$, it possesses a T symmetry at room temperature and finally transforms to a cubic phase above 300°C. For the sample with $x = 0.03$, it has an R structure at room temperature and changes to a weak T phase at 50°C; a further increase of temperature leads to the decline of tetragonality and finally makes it become a cubic.

However, for the sample with $x = 0.05$ no trace of T phases can be detected with increasing temperature. Therefore, it was demonstrated that the addition of BZ tends to stabilize low-temperature R phase.

Raman spectroscopy has proved to be an effective way to characterize the phase structure. Figure 1(g) shows the Raman spectra of the sample with $x = 0.025$ in the temperature range of −180° to 200°C. According to the Last's theory, the intermediate and high-frequency vibrations are correlated with NbO_6 octahedra, consisting of $\nu_1(A_{1g})$, $\nu_2(E_g)$, $\nu_3(F_{1u})$, $\nu_4(F_{1u})$, $\nu_5(F_{2g})$, and $\nu_6(F_{2u})$ in the range of 200–900 cm^{-1}.[15] Because of the random grain orientation in the ceramics, the Raman lines are relatively broad compared with a single crystal owing to the mode mixing and long-range force effects.[16] However, considering that the peak shift for the ν_1 stretching mode usually possesses a discontinuity during phase transition, a plot of Raman shift ν_1 versus temperature is shown in Fig. 1(h) by analyzing spectra with Lorentz-type peak functions. The peak shift to a low frequency is due to the softness of binding strength caused by the increase of temperature and exhibits an obvious discontinuity corresponding to R–T phase transition and T–C phase transition, respectively. It is important to note that the R–T phase transition was located near room temperature for the sample with $x = 0.025$.

Table I. Refined Structural Parameters by Using the Rietveld Method for NKNS–LT–xBZ Ceramics

x	0	0.01	0.02		0.025		0.03	0.04	0.05	0.06	0.08
a' (Å)	3.9477	3.9494	3.9526	3.9524	3.9689	3.9559	3.9641	3.9706	3.9756	3.9789	3.9872
b' (Å)	3.9477	3.9494	3.9526	3.9524	3.9689	3.9559	3.9641	3.9706	3.9756	3.9789	3.9872
c' (Å)	3.9922	3.9855	3.9855	3.9524	3.9822	3.9559	3.9641	3.9706	3.9756	3.9789	3.9872
SG	$P4mm$	$P4mm$	$P4mm$	$R3m$	$P4mm$	$R3m$	$R3m$	$R3m$	$R3m$	$R3m$	$R3m$
R_{wp}	7.61	7.79	8.25	8.45	8.38	8.47	8.59	7.88	7.58	7.53	7.77
S	1.32	1.35	1.38	1.34	1.42	1.40	1.44	1.37	1.28	1.31	1.36
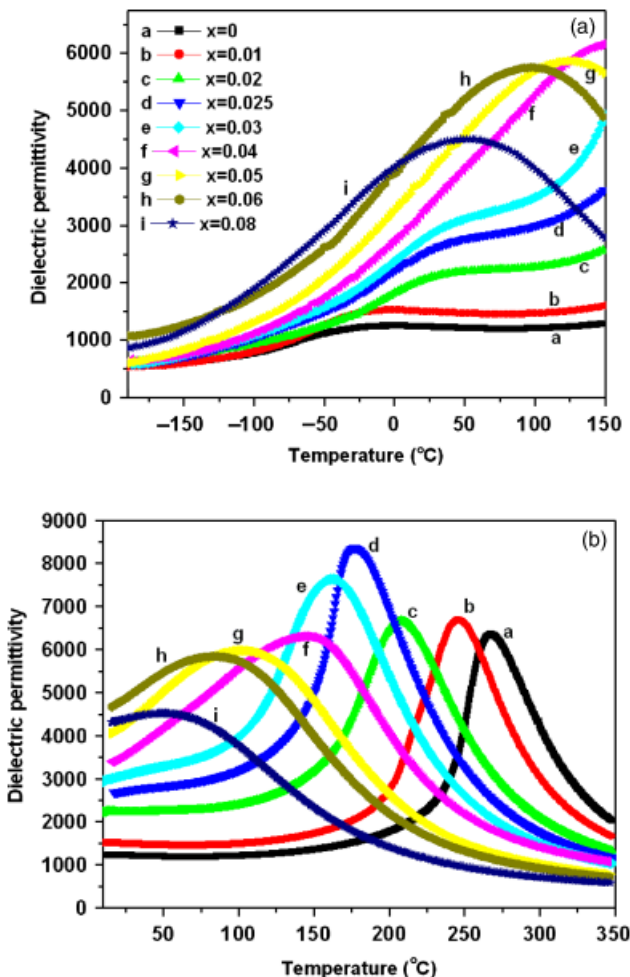
Fig. 2. Dielectric constant at 1 kHz as a function of temperature during heating for NKNS–LT–xBZ ceramics sintered at optimum temperature: (a) −150° to 150°C and (b) room temperature to 350°C (x as indicated).

The dielectric permittivity versus temperature curves for un-poled NKNS–LT–xBZ ceramics are shown in Fig. 2. The Curie temperature T_c, almost linearly decreases with x as seen from Fig. 2(b), but it is still above room temperature, further indicating that the sample with higher x (for example, $x = 0.05$) is a ferroelectric R phase rather than a paraelectric C phase. Figure 2(a) shows the change of PPT temperatures with x, although the nature of PPT can not be identified here. In association with XRD and Raman data, it can be determined that with the addition of BZ, the O–T phase transition changes to the R–T phase transition at $x \sim 0.02$, basically owing to the shrinkage of O phase zone. Recent studies indicated that the addition of LT can stabilize the T phase of NKN.[3–6] Although the tetragonality is commonly associated with the tolerance factor,[17] it was yet pointed out that the increased tetragonality can be also achieved by introducing smaller A-site ions such as Li⁺ in some perovskite materials such as alkaline niobates,[18] which restrain the rotational instabilities owing to the frustration between large A-site ions and small Li⁺ and presents A-site driven rather than B-site driven ferroelectricity[19–21] based on larger off-centering of Li⁺, thus inducing strong anisotropy and stabilizing the tetragonal state.[18] Unlike T phase, the R state is driven entirely by B sites such as in Pb(Zr,Ti)O₃ and Ba(Zr,Ti)O₃ where there exist B-site cation disorder and simple interatomic actions.[22] Moreover, the substitution of smaller B-site cations (i.e., Ta⁵⁺) with larger Zr⁴⁺ ions tends to produce negative physical pressure which favors low-temperature phase structures as well.[23,24]

According to the above results, a temperature–composition phase diagram of NKNS–LT–xBZ system within a certain range of BZ content was proposed as shown in Fig. 3. The
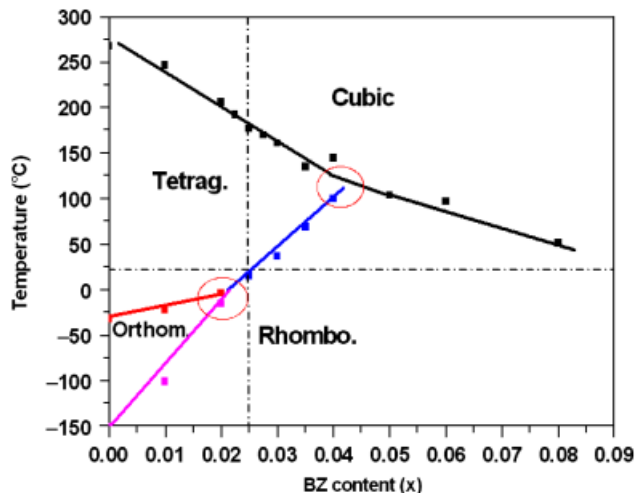
Fig. 3. Diagram of phase transition temperature versus composition for pseudo-ternary NKNS–LT–xBZ system derived from the dielectric constant, X-ray diffraction patterns together with Raman spectroscopy.

phase diagram is characterized by a phase boundary line separating ferroelectric T and R phases and locating between two trifurcate points (R–O–T triple point and R–C–T triple point) at $x \sim 0.02$ and $T \sim -5$°C, and at $x \sim 0.04$ and $T \sim 115$°C, respectively, as marked by two circles. The existence of two triple points could make NKNS–LT–xBZ system different from most of non-Pb systems, but look somewhat like (Ba,Ca)(Ti,Zr)O₃ system in which one triple point was reported.[14] Moreover, it can be seen that the sample with x close to 0.025 exhibits the R–T phase coexistence near room temperature. However, it is still unclear whether the R–T phase boundary is an MPB typical for Pb-based systems, or still a PPB usually for NKN-based compositions with O–T phase coexistence.[13] Further study on this issue is under progress. It has been noted that the existence of R–C–T triple point characterizes many highly piezoelectric Pb-based systems such as PZT and PMN–PT.[25] It should be anticipated that R–O–T triple point may also contribute to the piezoelectric performance.

P–E hysteresis loops of NKNS–LT–xBZ ceramics sintered at optimum temperatures are shown in Fig. 4. It can be seen that both coercive field E_c and remanent polarization P_r decline with the substitution of BZ for LT. It is obvious that the T phase dominating in 90° domains generally has higher E_c values than the R phase. However, at $x = 0.025$, E_c decreases sharply but P_r remains high values because the R–T phase coexistence causes
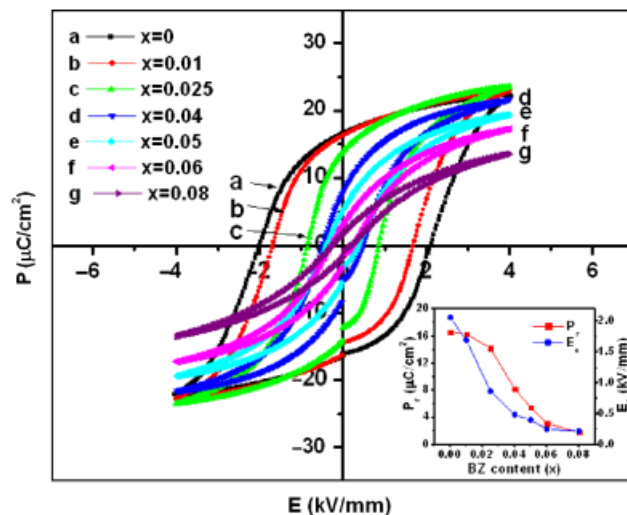
Fig. 4. Polarization versus electric field hysteresis loops of NKNS–LT–xBZ ceramics sintered at optimum temperature; Insets are the curves of remnant polarization P_r and coercive field E_c versus the BZ content.
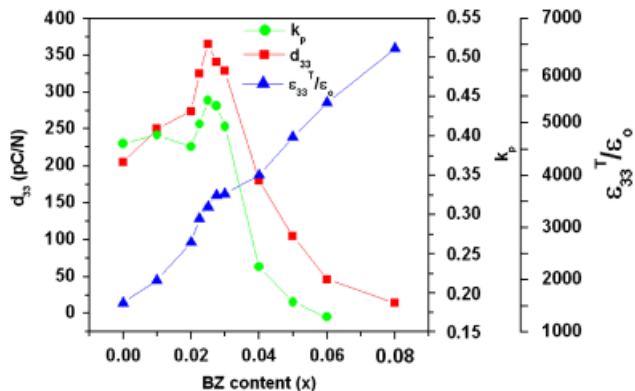
Fig. 5. Composition dependence of various electrical properties of poled NKNS–LT–xBZ ceramics.

the instability of the polarization state, probably plus the proximity to two triple points and the decreased tetragonality, such that the polarization direction can be easily rotated by external electric fields.

Dielectric and piezoelectric properties of poled NKNS–LT–BZ ceramics are shown in Fig. 5. It is shown that piezoelectric and electromechanical properties exhibit optimum values of $d_{33} = 365$ pC/N and $k_p = 45\%$ at $x = 0.025$ where the R–T ferroelectric phases coexist. However, both values decrease sharply with the addition of more BZ mainly owing to the weakening ferroelectricity, although the dielectric permittivity $\varepsilon_{33}^T/\varepsilon_o$ increases nearly linearly with the addition of BZ. The increased dielectric permittivity is mainly ascribed to the decrease of T_c and the enhanced diffuseness of T–C ferroelectric phase transition.

IV. Conclusions

Pseudo-ternary lead-free piezoelectric system NKNS–LT–xBZ was reported, which exhibits excellent piezoelectric properties in the proximity of the R–T phase coexistence zone. A temperature–composition phase diagram was proposed in which an R–T phase boundary line linking R–O–T and R–C–T triple points at two ends is formed near room temperature. Reduced energy barriers for polarization rotation for compositions with $x \sim 0.025$ could contribute to the enhancement of piezoelectric properties ($d_{33} = 365$ pC/N and $k_p = 45\%$). Our work may provide a new method for designing high-performance piezoelectric materials.

References

[1]H. J. Trodahl, N. Klein, D. Damjanovic, N. Setter, B. Ludbrook, D. Rytz, and M. Kuball, "Raman Spectroscopy of (K,Na)NbO$_3$ and (K,Na)$_{1-x}$Li$_x$NbO$_3$," *Appl. Phys. Lett.*, **93**, 262901 (2008).

[2]B. Jaffe, W. R. Cook, and H. Jaffe, *Piezoelectric Ceramics.* Academic Press, New York, 1971.

[3]Y. Saito, H. Takao, T. Tani, T. Nonoyama, K. Takatori, T. Homma, T. Nagaya, and M. Nakamura, "Lead-Free Piezoceramics," *Nature*, **432**, 84–7 (2004).

[4]Y. P. Guo, K. Kakimoto, and H. Ohsato, "Phase Transitional Behavior and Piezoelectric Properties of (Na$_{0.5}$K$_{0.5}$)NbO$_3$–LiNbO$_3$ Ceramics," *Appl. Phys. Lett.*, **85**, 4121–3 (2004).

[5]E. Hollenstein, M. Davis, D. Damjanovic, and N. Setter, "Piezoelectric Properties of Li- and Ta-Modified (K$_{0.5}$Na$_{0.5}$)NbO$_3$ Ceramics," *Appl. Phys. Lett.*, **87**, 182905 (2005).

[6]D. M. Lin, K. W. Kwok, K. H. Lam, and H. L. W. Chan, "Structure, Piezoelectric and Ferroelectric Properties of Li- and Sb-Modified K$_{0.5}$Na$_{0.5}$NbO$_3$ Lead-Free Ceramics," *J. Phys. D: Appl. Phys.*, **40**, 3500–5 (2007).

[7]R. Z. Zuo, X. S. Fang, and C. Ye, "Phase Structure and Electrical Properties of New Lead-Free (Na$_{0.5}$K$_{0.5}$)NbO$_3$–(Bi$_{0.5}$Na$_{0.5}$)TiO$_3$ Ceramics," *Appl. Phys. Lett.*, **90**, 092904 (2007).

[8]R. Z. Zuo, X. S. Fang, and C. Ye, "Phase Transitional Behavior and Piezoelectric Properties of Lead-Free (Na$_{0.5}$K$_{0.5}$)NbO$_3$– (Bi$_{0.5}$K$_{0.5}$)TiO$_3$ Ceramics," *J. Am. Ceram. Soc.*, **90**, 2424–8 (2007).

[9]H. L. Du, W. C. Zhou, F. Luo, D. M. Zhu, S. B. Qu, Y. Li, and Z. B. Pei, "Design and Electrical Properties' Investigation of (K$_{0.5}$Na$_{0.5}$)NbO$_3$–BiMeO$_3$ Lead-Free Piezoelectric Ceramics," *J. Appl. Phys.*, **104**, 034104 (2008).

[10]R. P. Wang, H. Bando, and M. Itoh, "Universality in Phase Diagram of (K,Na)NbO$_3$–MTiO$_3$ Solid Solutions," *Appl. Phys. Lett.*, **95**, 092905 (2009).

[11]R. P. Wang, H. Bando, T. Katsumata, Y. Inaguma, H. Taniguchi, and M. Itoh, "Tuning the Orthorhombic–Rhombohedral Phase Transition Temperature in Sodium Potassium Niobate by Incorporating Barium Zirconate," *Phys. Status Solidi RRL*, **3**, 142–4 (2009).

[12]R. Z. Zuo, J. Fu, D. Y. Lv, and Y. Liu, "Antimony Tuned Rhombohedral–Orthorhombic Phase Transition and Enhanced Piezoelectric Properties in Sodium Potassium Niobate," *J. Am. Ceram. Soc.*, **93**, 2783–7 (2010).

[13]R. Z. Zuo, J. Fu, and D. Y. Lv, "Phase Transformation and Tunable Piezoelectric Properties of Lead-Free (Na$_{0.52}$K$_{0.48-x}$Li$_x$)(Nb$_{1-x-y}$Sb$_y$Ta$_x$)O$_3$ System," *J. Am. Ceram. Soc.*, **92**, 283–5 (2009).

[14]W. F. Liu and X. B. Ren, "Large Piezoelectric Effect in Pb-Free Ceramics," *Phys. Rev. Lett.*, **103**, 257602 (2009).

[15]S. D. Ross, "The Vibrational Spectra of Lithium Niobate, Barium Sodium Niobate and Barium Sodium Tantalate," *J. Phys. C: Solid State Phys.*, **3**, 1785–90 (1970).

[16]J. A. B. Saip, E. R. Moor, and A. L. Cabrera, "Raman Study of Phase Transitions in KNbO3," *Solid State Commun.*, **135**, 367–72 (2005).

[17]M. R. Suchomel and P. K. Davies, "Predicting the Position of the Morphotropic Phase Boundary in High Temperature PbTiO$_3$–Bi(B′B″)O$_3$ Based Dielectric Ceramics," *J. Appl. Phys.*, **96**, 4405–10 (2004).

[18]D. I. Bilc and D. J. Singh, "Frustration of Tilts and A-Site Driven Ferroelectricity in KNbO$_3$–NaNbO$_3$ Alloy," *Phys. Rev. Lett.*, **96**, 147602 (2006).

[19]M. R. Suchomel and P. K. Davies, "Enhanced Tetragonality in (x)PbTiO$_3$–$(1-x)$Bi(Zn$_{1/2}$Ti$_{1/2}$)O$_3$ and Related Solid Solution System," *Appl. Phys. Lett.*, **86**, 262905 (2005).

[20]D. M. Stein, M. R. Suchomel, and P. K. Davies, "Enhanced Tetragonality in (x)PbTiO$_3$–$(1-x)$Bi(B′B″)O$_3$ Systems: Bi(Zn$_{3/4}$W$_{1/4}$)O$_3$," *Appl. Phys. Lett.*, **89**, 132907 (2006).

[21]A. K. Kalyani, R. Garg, and R. Ranjan, "Competing A-Site and B-Site Driven Ferroelectric Instabilities in the $(1-x)$PbTiO$_3$–(x)BiAlO$_3$ System," *Appl. Phys. Lett.*, **94**, 202903 (2009).

[22]M. Ghita and M. Fornari, "Interplay Between A-Site and B-Site Drien Instabilities in Perovskites," *Phys. Rev. B*, **72**, 054114 (2005).

[23]R. Wordenweber, E. Hollmann, R. Kutzner, and J. Schubert, "Induced Ferroelectricity in Strained Epitaxial SrTiO$_3$ Films on Various Substrates," *J. Appl. Phys.*, **102**, 044119 (2007).

[24]W. Zhang, D. Vanderbilt, and K. M. Rabe, "First-Principles Theory of Ferroelectric Phase Transitions for Perovskites: The Case of BaTiO$_3$," *Phys. Rev. B*, **52**, 6301–12 (1995).

[25]D. E. Cox, B. Noheda, G. Shirane, Y. Uesu, K. Fujishiro, and Y. Yamada, "Universal Phase Diagram for High-Piezoelectric Perovskite Systems," *Appl. Phys. Lett.*, **79**, 400–3 (2001).   □